Cell

Cancer-Associated PTEN Mutants Act in a Dominant-Negative Manner to Suppress PTEN Protein Function

Antonella Papa,[1] Lixin Wan,[2] Massimo Bonora,[3] Leonardo Salmena,[1,6] Min Sup Song,[1,7] Robin M. Hobbs,[1,8] Andrea Lunardi,[1] Kaitlyn Webster,[1] Christopher Ng,[1] Ryan H. Newton,[4,9] Nicholas Knoblauch,[2] Jlenia Guarnerio,[1] Keisuke Ito,[1,10] Laurence A. Turka,[4,9] Andy H. Beck,[2] Paolo Pinton,[3] Roderick T. Bronson,[5] Wenyi Wei,[2] and Pier Paolo Pandolfi[1,*]

[1]Cancer Research Institute, Beth Israel Deaconess Cancer Center, Department of Medicine and Pathology, Beth Israel Deaconess Medical Center, Harvard Medical School, Boston, MA 02215, USA
[2]Department of Pathology, Beth Israel Deaconess Medical Center, Harvard Medical School, Boston, MA 02115, USA
[3]Department of Morphology, Surgery and Experimental Medicine Section of General Pathology University of Ferrara, Ferrara 44124, Italy
[4]Department of Medicine, Beth Israel Deaconess Medical Center, Harvard Medical School, Boston, MA 02115, USA
[5]Department of Microbiology and Immunobiology, Harvard Medical School, Boston, MA 02115, USA
[6]Present address: Department of Pharmacology and Toxicology, University of Toronto and Princess Margaret Cancer Centre, Toronto, ON M5G 2M9, Canada
[7]Present address: Department of Molecular and Cellular Oncology, MD Anderson Cancer Center, 1515 Holcombe Boulevard, Houston, TX 77037, USA
[8]Present address: Australian Regenerative Medicine Institute and Department of Anatomy and Developmental Biology, Monash University, Clayton, VIC 3800, Australia
[9]Present address: Department of Surgery, Transplantation Biology Research Center, Massachusetts General Hospital, Harvard Medical School, Boston, MA 02114, USA
[10]Present address: Ruth L. and David S. Gottesman Institute for Stem Cell and Regenerative Medicine Research and Departments of Medicine and Cell Biology, Albert Einstein Cancer Center, Albert Einstein College of Medicine, Bronx, NY 10461, USA
*Correspondence: ppandolf@bidmc.harvard.edu
http://dx.doi.org/10.1016/j.cell.2014.03.027

SUMMARY

PTEN dysfunction plays a crucial role in the pathogenesis of hereditary and sporadic cancers. Here, we show that PTEN homodimerizes and, in this active conformation, exerts lipid phosphatase activity on PtdIns(3,4,5)P_3. We demonstrate that catalytically inactive cancer-associated PTEN mutants heterodimerize with wild-type PTEN and constrain its phosphatase activity in a dominant-negative manner. To study the consequences of homo- and heterodimerization of wild-type and mutant PTEN in vivo, we generated *Pten* knockin mice harboring two cancer-associated PTEN mutations (PtenC124S and PtenG129E). Heterozygous $Pten^{C124S/+}$ and $Pten^{G129E/+}$ cells and tissues exhibit increased sensitivity to PI3-K/Akt activation compared to wild-type and $Pten^{+/-}$ counterparts, whereas this difference is no longer apparent between $Pten^{C124S/-}$ and $Pten^{-/-}$ cells. Notably, *Pten* KI mice are more tumor prone and display features reminiscent of complete *Pten* loss. Our findings reveal that *PTEN* loss and PTEN mutations are not synonymous and define a working model for the function and regulation of PTEN.

INTRODUCTION

Phosphatase and tensin homolog deleted on chromosome ten (*PTEN*) is a tumor suppressor frequently lost or mutated in human cancers and in a number of tumor syndromes, referred to as "PTEN hamartoma tumor syndromes" (PHTS), which include Cowden disease (CD) and Bannayan-Zonana syndrome (Hollander et al., 2011).

To study the consequences of Pten loss in vivo, we and others generated animal models with partial and total loss of *Pten* (Di Cristofano et al., 1998; Podsypanina et al., 1999; Suzuki et al., 1998). Total *Pten* loss was found to lead to embryonic lethality, and additional investigations in a hypomorphic allelic series of mice with sequentially lower *Pten* expression revealed that even small reductions in *Pten* doses can elicit cancer phenotypes (Alimonti et al., 2010; Trotman et al., 2003). Conversely, systemic elevation of *Pten* through transgenic overexpression results in a constitutively augmented tumor-suppressive state (Garcia-Cao et al., 2012).

PTEN functions as a dual-specificity protein phosphatase (DSP) with predominant enzymatic activity on phosphoinositides (Maehama and Dixon, 1998). As a phospholipid phosphatase, PTEN catalyzes the hydrolysis of the second messenger PtdIns (3,4,5)P_3 (PIP3) and counteracts the activation of the PI3K/AKT pathway, thus regulating cellular growth, proliferation, and metabolism (Maehama and Dixon, 1998).

In line with its protein phosphatase function, PTEN has been shown to dephosphorylate phosphopeptides in vitro (Myers

et al., 1998), and reported phosphoprotein targets include the focal adhesion kinase, c-SRC, as well as PTEN itself (Tamura et al., 1999; Tibarewal et al., 2012; Zhang et al., 2011).

Heterozygous deletion of *Pten* in mice faithfully phenocopies biological features found in many human tumors with partial loss of *PTEN* (Di Cristofano et al., 1998). However, reports indicate that genetic loss of *PTEN* and mutations leading to PTEN loss of function may not be equivalent. For instance, Marsh et al. (1998) reported a genotype-phenotype correlation in patients diagnosed with CD who developed several tumors, including breast tumors. Importantly, they found that patients harboring missense *PTEN* mutations in the phosphatase core developed higher numbers of lesions than patients with truncating mutations (Marsh et al., 1998). This led us to hypothesize that expression of catalytically inactive mutant PTEN enzyme may be more unfavorable than PTEN protein loss.

Regulation of PTEN function occurs through various posttranslational modifications implicated in PTEN membrane recruitment, subcellular localization, or protein-protein interactions (Wang and Jiang, 2008). Structurally, PTEN belongs to the Class I Cys-based protein tyrosine phosphatase (PTP) and, more specifically, to the VH1-like family (Alonso et al., 2004). PTEN contains an N-terminal phosphatase domain with a conserved active site; a C-terminal C2 domain followed by two PEST sequences and a PDZ-binding domain (Lee et al., 1999). It has been reported that PTEN interacts with a number of PDZ-domain bearing proteins to achieve higher levels of complex formation (Sotelo et al., 2012; Vazquez et al., 2001). We therefore hypothesized, and have here demonstrated, that PTEN can interact with itself. We show that dimer PTEN is active toward its phosphoinositide substrate PIP3 and thereby inhibits the activation of the PI3K/AKT signaling pathway. Critically, we find that in a dimeric conformation, cancer-associated missense mutations have dominant-negative consequences over wild-type (WT) protein function, with ensuing implications for tumorigenesis.

RESULTS

PTEN Exists in a Dimeric Complex

Given that VH1-like phosphatases are known to exist in higher order complexes/dimers (Koksal and Cingolani, 2011), we examined whether PTEN could form similar complexes. For this, we performed coimmunoprecipitation (co-IP) experiments using the *PTEN* null cell line PC3. By cotransfecting differentially tagged PTEN variants we were able to reciprocally co-IP GFPPTEN and MycPTEN (Figure 1A). Moreover, in 293T cells overexpressing GFPPTEN, we were able to co-IP endogenous PTEN (Figure 1B).

Monomeric PTEN has a molecular weight of 50–55 kDa in denaturing conditions. If a dimeric PTEN existed, it would migrate at double that size in nonreducing and nondenaturing SDS-PAGE. Accordingly, immunoprecipitation (IP) and native elution of MycPTEN from transfected PC3 cells revealed the presence of two bands consistent with the monomeric and dimeric status of the protein (100 kDa circa) (Figure S1A available online). To control for overexpression artifacts, we repeated this assay by pulling down endogenous Pten in NIH 3T3 and confirmed the presence of two bands (Figure 1C).

Next, we investigated the contribution of covalent and noncovalent interactions to dimer formation and found that disulfide bonds are not a major requirement for the stabilization of this interaction (Figure S1B). We also verified PTEN homodimerization in vitro by coexpressing GST-PTEN and His-PTEN in bacteria. In these experiments, we successfully recovered His-PTEN in GST-PTEN pull-downs (Figure 1D).

To further validate the direct binding between PTEN molecules in a eukaryotic system, we employed bioluminescence resonance energy transfer (BRET). To this end, we used *Renilla* luciferase-PTEN (PTENRluc) as energy donor and GFPPTEN as energy acceptor (Figure 1E); coelenterazine was used as substrate for the luciferase. Coexpression of PTENRluc with GFPPTEN generated a significant increase in the total BRET signal compared to empty GFP, with GFP emission only occurring when in close proximity (<100 Å) to the luminescent PTENRluc (Figure 1F). We also performed competition assays. Coexpression of donor and acceptor proteins with increasing doses of untagged PTEN showed a reduction of net BRET, providing further evidence of direct PTEN-PTEN interaction (Figure 1G).

Finally, we sought to determine whether PTEN dimerization occurs in both the nucleus and cytoplasm. Utilizing BRET, we found no variations in nuclear emission over the total BRET signal, neither in basal conditions nor upon serum stimulation, suggesting that PTEN dimer likely exists in both compartments (Figure 1H). This finding was confirmed in co-IPs performed upon nuclear versus cytoplasmic fractionation (Figures S1C and S1D). Thus, we have demonstrated by multiple approaches that PTEN can exist in a homodimeric complex.

PTEN Dimer Is Catalytically Active

To identify the protein domains responsible for PTEN dimer formation, we generated GST-fusion proteins with PTEN N terminus (GST-PTENΔC terminus) and PTEN C terminus domains (GST-PTENΔN terminus) (Figure 2A). Coexpression of GST-PTEN full length (FL) with His-PTENFL confirmed the interaction between the two FL proteins (Figure 2B). Notably, His-PTENFL was pulled down by both GST-PTEN-domains in bacteria (Figure 2B). We then tested the binding by co-IPs in PC3 cells and confirmed that in eukaryotic cells PTEN uses multiple interfaces along the entire protein to achieve a dimeric conformation (Figures S2A and S2B).

To corroborate these findings, we tested the ability of different PTEN domains to homodimerize in vivo (Figure 2C). In nonreducing SDS-PAGE, total lysates from PC3 cells transfected with MycPTENFL, MycPTENΔN terminus, or MycPTENΔPDZ revealed the appearance of upper bands at twice the size of the respective monomeric proteins. Strikingly, upon stabilization of MycPTENΔC terminus and MycPTENΔCTD with the protease inhibitor MG132, we observed dimeric bands with all PTEN variants tested (Figure 2D), with the MycPTENΔC terminus showing the highest propensity to self-associate (Figure 2E). Notably, the MycPTENΔC terminus and MycPTENΔN terminus exhibited a potential to oligomerize, as evidenced by additional higher molecular weight bands (Figure 2D, asterisks).

We also studied binding directionality and found that while in a closed head-to-tail monomeric conformation PTEN is inactive toward its lipid substrate (Leslie and Foti, 2011), through

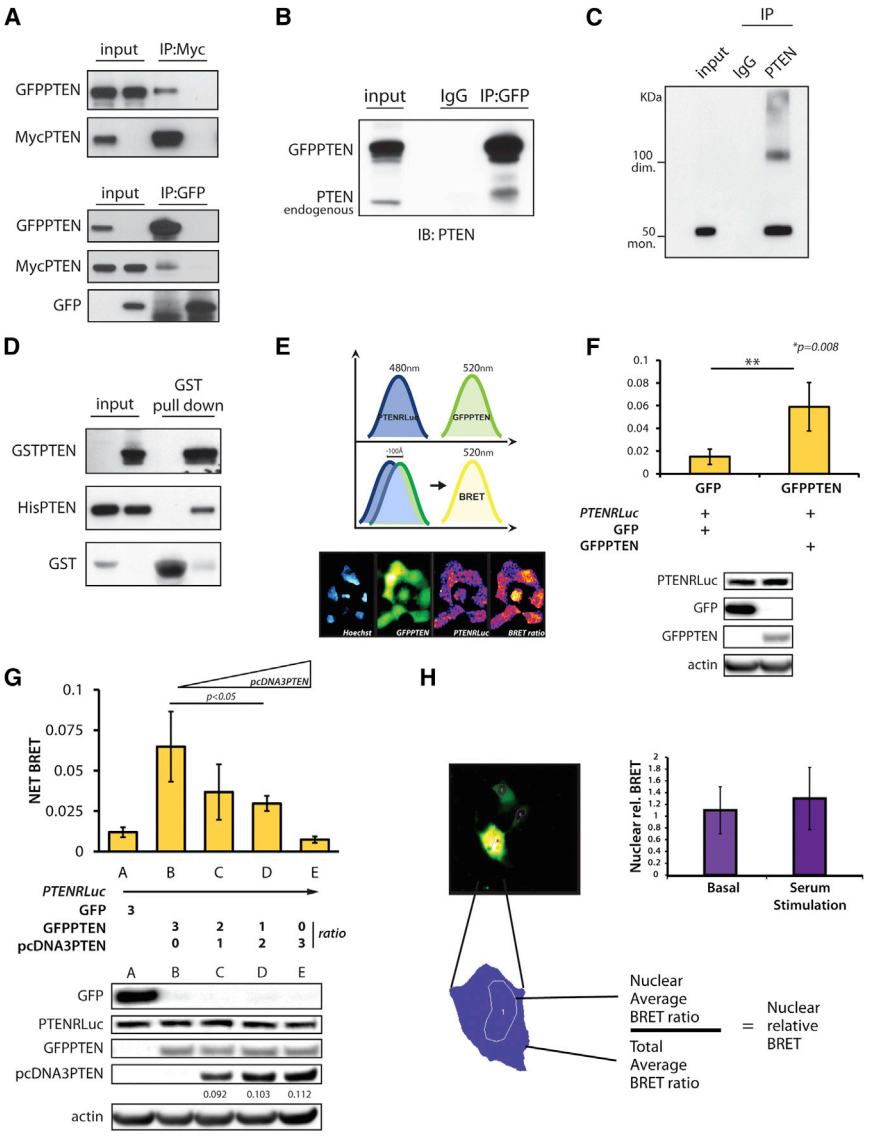

Figure 1. PTEN Exists in a Dimeric Complex

(A) Co-IPs from total lysate of PC3 cells. IP of MycPTEN (top) and IP of GFPPTEN (bottom) with specific tag antibodies revealed reciprocal PTEN-PTEN interaction.

(B) Co-IPs from total lysate of 293T cells, transfected with GFPPTENWT and IP with anti-GFP antibody. Western blot was probed with a PTEN antibody.

(C) NIH 3T3 cell lysates were IP with anti-rabbit PTEN antibody; native elution and western blots show monomer and dimer of the protein using mouse anti-PTEN antibody.

(D) In bacteria, GST-PTEN specifically pulls down His-PTEN.

(E) Renilla and GFP emissions are detected at the indicated wavelengths. Administration of Coelenterazine induces Renilla excitation that generates BRET signal when in proximity to the GFP. Bottom: images of fluorescent signals generated by the different chimeras.

(F) Detection of PTEN-PTEN interaction by BRET in PC3 cells transfected with the indicated plasmids. Bottom shows expression levels of the different chimeras. Mean values with associated SD are shown.

(G) Competition assays performed by BRET. Bottom: expression levels of the indicated chimeras. Quantification of Un-tagged PTEN cloned in the pcDNA3.1 vector is normalized to β-actin. Mean values with associated SD are shown.

(H) In PC3, BRET signal is collected in a single cell fashion and nuclear emission normalized over average of total emission. Mean values with relative SD are shown.

See also Figure S1.

head-to-head intermolecular binding, it achieves a more active enzymatic conformation (Figures S2C–S2F).

We next tested the catalytic activity of antibody-purified PTEN dimers from PC3 cells. PTENFL displayed different affinities toward PTEN deletion mutant versions (Figure S2B), and higher levels of dimerization between PTENFL and PTEN domains correlated with higher levels of free phosphate release (Figure S2E).

We likewise performed gel filtration of various PTEN species followed by phosphatase assays using PIP3 as substrate. Total lysates of HEK293 cells with exogenous MycPTEN expression were fractioned and a low molecular weight range (30–160 kDa) identified by western blot analysis (Figures 2F, top, and S2G). Importantly, eluted fractions corresponding to dimeric PTEN (fractions 26–27) generated higher phosphate release than fractions of a lower molecular weight which contained monomeric PTEN (fractions 28–29) (Figure 2G). Thus, we conclude that PTEN dimerization defines a more active complex with respect to the less active PTEN monomer.

Phosphorylation of the PTEN Tail Regulates PTEN Dimerization

Next, we studied the conformational status of PTEN by gel filtration analyses. FLAG-tagged PTEN without the C-terminal tail (FlagPTENΔCTD) was expressed in HEK293 cells and total lysates were fractioned. Western blot analysis revealed a striking upward shift of tail-less PTEN compared to PTENFL, indicating an enriched dimeric status (Figure 2F).

Because the physiologic role of the PTEN tail is mediated by its phosphorylation status (Vazquez et al., 2000), we performed gel filtration analyses by using phosphomimetic and phosphodead mutant-tail versions of PTEN. We focused specifically on amino acids S380, T382, T383, and S385. By expressing nonphosphorylatable PTEN (PTEN S380A, T382A, T383A, S385A: PTEN4A) we functionally mimicked deletion of the PTEN C-terminal tail. Notably, the PTEN4A presented the same upward shift we found with expression of PTENΔCTD (Figure 2F). In contrast, expression of a phosphomimetic PTEN (PTEN4E) prevented this shift, indicating a possible role for PTEN tail-phosphorylation in governing its dimeric status (Figure 2F).

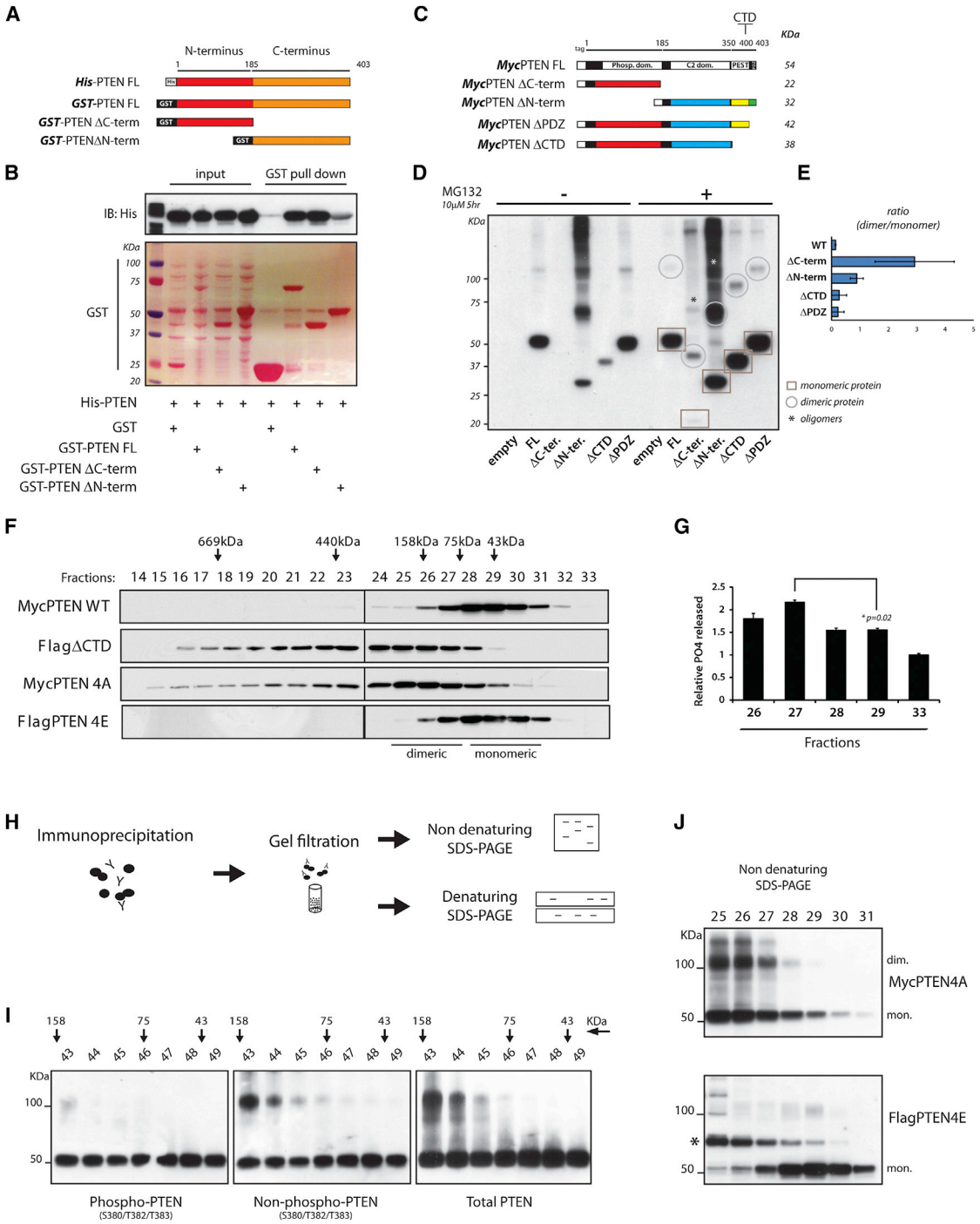

Figure 2. Dimerization Defines a Pool of Catalytically Active PTEN

(A) Diagram of recombinant proteins showing PTEN FL and deletion mutants. In red, N terminus domain, amino acid (aa) 1–185; in orange, C terminus domain, aa 186–403.

(B) GST-PTENFL and domains were purified (Ponceau-S staining); His-PTEN pulled down is detected by western blot.

(C) Schematic representing series of Myc-tagged PTENFL and deletion mutant vectors. Predicted molecular weights are indicated.

(D) PC3 cells were transfected with the indicated expression vectors. Total lysates were resolved by nonreducing SDS-PAGE and probed with an anti-Myc antibody. Circles and squares indicate monomeric and dimeric PTEN conformations, respectively. Asterisks indicate oligomers of PTEN domains.

(E) Ratio between PTEN dimer/monomer in PTEN FL and deletion mutant series. Average of three independent experiments is shown with associated SD.

(F) Lysates from HEK293 cells transfected with the indicated PTEN vectors were separated by gel filtration. Fractions were resolved by SDS-PAGE and probed with specific tag antibodies.

(legend continued on next page)

Next, we assessed the phosphorylation level of PTEN dimer. To this end, we immunopurified PTEN and eluted the complex in nonreducing conditions. After tandem-column gel filtrations we analyzed the immunocomplex by reducing and nonreducing SDS-PAGE (Figure 2H). In reducing SDS-PAGE, immunopurified PTENFL appeared in two peaks corresponding to a "low-" and a "high-molecular-weight complex" (Figure S2H). We then tested the phospho/nonphospho status of the dimeric PTEN in nonreducing SDS-PAGE. First, with a total PTEN antibody we confirmed the presence of PTEN as a monomer and dimer (Figure 2I, right). Importantly, we found that while a specific "phospho-PTEN" antibody only recognizes the monomeric form, the relative "nonphospho" PTEN showed the appearance of both monomeric and dimeric protein (Figure 2I, left and middle).

Finally, we tested total lysates from HEK293 cells expressing PTEN4A and PTEN4E. Here, we found that while PTEN4E only runs as a single monomeric band (Figure 2J, bottom), PTEN4A showed monomeric and dimeric PTEN conformations (Figure 2J, top), in agreement with the shift found by gel filtration. Thus we demonstrate that phosphorylation of the C-terminal tail maintains PTEN as a monomer, whereas the absence of phosphorylation is associated with a dimeric conformation.

PTEN Cancer-Associated Mutations Exert Dominant-Negative Effects over Wild-Type Protein

We then asked if mutant PTEN protein could form dimers and whether mutations altered dimer formation or activity. The most studied cancer-associated PTEN mutations are the Cys-124 to Ser (C124S) and the Gly-129 to Glu (G129E). C124S mutation generates a catalytically dead PTEN variant that is associated with endometrial cancer and is reported to completely ablate PTEN phosphatase activity (Bonneau and Longy, 2000; Myers et al., 1997), whereas the G129E mutation is associated with CD and abrogates the phosphoinositide phosphatase function but retains activity toward phosphopeptides (Liaw et al., 1997; Myers et al., 1998). Both mutations lie in the PTEN catalytic core.

To test our hypothesis, we first analyzed the ability of MycPTENC124S and MycPTENG129E to homodimerize. In nonreducing conditions, we found that both mutants appear as monomers and dimers, like the wild-type protein (Figure 3A). PTEN mutants were also able to form heterodimers with wild-type PTEN as found in our co-IP experiments (Figure 3B). BRET experiments further demonstrated that PTENWT-Rluc interacted with either GFPPTEN-C124S or G129E (Figure 3C).

In bacteria, GST pull-down experiments confirmed that His-PTENWT binds both GST-tagged PTEN mutants (Figure 3D). Importantly, purified heterodimers were tested for phosphatase activity on PIP3. In control experiments, GST-PTENWT alone or a His-PTENWT:GST-PTENWT mix produced effective free phosphate release. However, heterodimers comprised of His-PTENWT:GSTPTENC124S or His-PTENWT:GSTPTENG129E had reduced capacity to hydrolyze PIP3 compared to GST-PTENWT (Figure 3E), leading us to consider the possibility that in a heterodimeric state, the catalytically inactive mutations inhibited activity of the wild-type PTEN protein toward PIP3, as we next demonstrated in vivo.

Generation and Characterization of *Pten* Knockin Mutant Mice

To investigate the physiological consequences of PTEN-PTEN mutant heterodimers, we generated mouse models expressing PTENC124S and PTENG129E (Figures S3A and S3B). For the $Pten^{C124S/+}$ and $Pten^{G129E/+}$ mouse models, we substituted T to A at position 370 or G to A in position 386 of *Pten* exon5, respectively (Figure 3F).

In performing the in vivo characterization of these new *Pten* KI mice, we also aimed to investigate two critical aspects of PTEN regulation: stability and localization. First, since many *PTEN* missense point mutations render PTEN unstable (Georgescu et al., 1999), we measured the mutant Pten proteins levels in our *Pten* KI mice. We observed that $Pten^{C124S/+}$ and $Pten^{G129E/+}$ express a total level of Pten that is comparable to levels in Pten wild-type mice (Figure 3G). Second, to exclude the contribution of defective cellular distribution to our analysis, we performed cell-fractionation and immunofluorescence (IF) analyses. Here, we found that $Pten^{C124S/+}$ and $Pten^{G129E/+}$ MEFs (Figures 3H–3J) displayed comparable Pten localization patterns to wild-type cells.

In Vivo Confirmation of the Dominant-Negative Functions of Mutant Pten

Because homozygous *Pten* loss is lethal in embryogenesis, we investigated the possibility of generating homozygous *Pten* KI mice. Three independent crosses per mutation failed to yield live pups with a homozygous mutant genotype, indicating that the lipid phosphatase activity of Pten is an essential function during embryogenesis (Figures S4A and S4B).

To evaluate the consequences of harboring loss-of-function Pten mutants in heterozygosity, we established cohorts of $Pten^{C124S/+}$, $Pten^{G129E/+}$, and $Pten^{+/-}$ mice as controls. Because *Pten* heterozygosity initiates neoplastic transformation of epithelial tissues and leads to severe lymphoproliferation (Di Cristofano et al., 1999), we collected a number of organ samples for histological analysis. We found that young mice between 8 and 16 weeks of age showed hyperplastic changes in the lymph nodes, with expansion of T cells (data not shown). Surprisingly, unlike $Pten^{+/-}$ mice, a significant number of $Pten^{C124S/+}$,

(G) Fractions containing different conformations of PTEN and collected as in (F) were tested for their activity toward PIP3 and normalized over protein levels. Mean values from triplicate wells with associated SD are shown.

(H) Experimental flow chart: cell lysates were subjected to IP with an anti-Myc antibody. Immunocomplexes were eluted in native conditions and separated by tandem-column gel filtration. See also Figure S2H. Collected fractions were resolved by reducing (Figure S2H) and nonreducing SDS-PAGE (I).

(I) Fractions collected as in (H) were resolved by nonreducing SDS-PAGE and probed with the indicated PTEN antibodies.

(J) Nonreducing SDS-PAGE of eluted fractions generated as in (F) were blotted with anti-Myc (top) and anti-Flag (bottom) antibodies. Asterisk indicates a shift in FlagPTEN4E probably due to posttranslational modifications.

See also Figure S2.

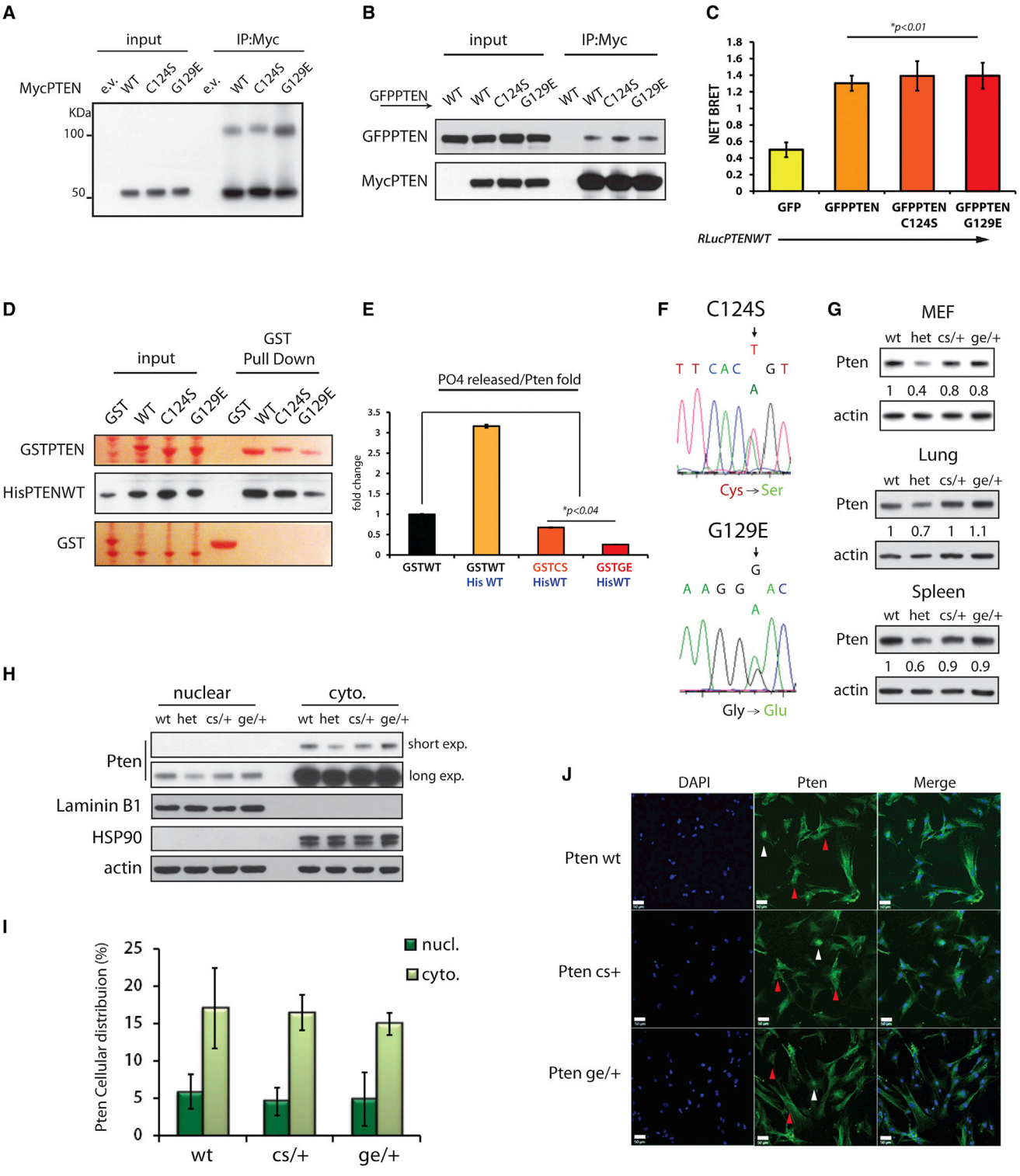

Figure 3. PTENC124S and PTENG129E Mutations Heterodimerize with PTEN Wild-Type and Inhibit Its Phosphatase Function

(A) Nonreducing SDS-PAGE of lysates from PC3 cells transfected with MycPTENWT or mutant vectors and IP with an anti-Myc antibody.

(B) IPs from PC3 cell lysates transfected with the indicated vectors were performed and western blots probed with an anti-PTEN antibody.

(C) BRET analysis on PC3 cells complemented with the indicated vectors. Mean values with associated SD are shown.

(D) GST-pull down (in Ponceau-S staining) reveals binding between prokaryotic PTEN WT and mutant versions. Western blots are probed with anti-His antibody.

(legend continued on next page)

Pten$^{G129E/+}$ mice developed lymphoproliferation features by 16 weeks (Figure S3E). Accordingly, older *Pten* KI mice had increased spleen weights, compared to *Pten*$^{+/-}$ mice, owing to severe extramedullary hematopoiesis and lymphoid hyperplasia; we also found extended expansion of white blood cells in the peripheral blood (Figure S3F). In solid tissues, the tumor spectrum of *Pten* KI mice was indistinguishable from *Pten*$^{+/-}$ mice, with lesions developing in several glands and organs (Figures S3C and S3D). However, histological assessments at different time points revealed that a greater proportion of *Pten* KI mice developed adenomas of the thyroid, adrenal, and gallbladder, with 2 out of 29 *Pten*$^{C124S/+}$, and 3 out of 37 *Pten*$^{G129E/+}$ male mice also developing invasive adenocarcinoma of the thyroid. In addition, three *Pten*$^{C124S/+}$ mice developed lung adenomas, and 4 out of 30 *Pten*$^{G129E/+}$ female mice developed liver adenomas, a lesion never observed in our *Pten*$^{+/-}$ mice (Figures S3C and S3D). In mammary tissues, 68.9% of our *Pten*$^{+/-}$ mice between 9 and 12 months developed hyperplastic lesions (13 out of 29, 44.8%) or small adenocarcinomas (7 out of 29, 24.1%). Lesions developed in 66% and 67% of *Pten*$^{C124S/+}$and *Pten*$^{G129E/+}$ mice, respectively; however, along with a number of hyperplasia cases and small adenocarcinomas (9 out of 27, 33.3%, for *Pten*$^{C124S/+}$, and 7 out of 24, 29.1%, for *Pten*$^{G129E/+}$) we also found that 33.3% of *Pten*$^{C124S/+}$ mice (9 out of 27) and 37.5% of *Pten*$^{G129E/+}$ mice (9 out of 24) developed large invasive adenocarcinomas (Figures 4A and 4B). Thoracic and inguinal fat pads presented massive expansion of epithelial cells and connective tissue, with central necrotic areas likely due to tumor size, which reached 0.6 cm^2 on average (Figures 4C and S4C).

As PTEN loss also leads to defects in neuronal development, we assessed the status of different neuronal populations (Fraser et al., 2004). Histopathological analysis revealed that only the pituitary gland presented signs of tumorigenesis, with adenomas developing primarily in the anterior lobe (Figure S4E) (Bai et al., 2006). However, in the cerebellum, we found that while *Pten*$^{+/-}$ mice had histologically normal brains, both *Pten* KI cohorts developed features of Lhermitte-Duclos disease, or "dysplastic gangliocytoma" (Figures 4D, 4E, S4D, and S4G) (Backman et al., 2001; Kwon et al., 2001). An average of 25% of *Pten*$^{C124S/+}$ and *Pten*$^{G129E/+}$ mice had enlarged areas in the cerebellum, with disorganized spreading of granule cells into the molecular layer, increased thickness of the molecular layer itself, and the presence of neurons expressing the neuronal marker, NeuN (Figure 4F). Immunostaining confirmed the expansion of glial cells (mostly astrocytes, GFAP positive, Figure 4F), together with an increased number and size of glial fibers, as shown by positivity to the proliferation marker PCNA (Figure S4F). Affected areas reshaped the structure of the cerebellar lobes and led to dispersion of the Purkinje cells in the molecular layer (Calbindin staining in Figure 4F). These "PHTS" features were found as early as 4 months of age and presented in small localized areas, as well as in more developed lesions that pervaded the whole cerebellum (Figure 4E). Notably, conditional loss of *Pten* in the brain, under Gfap-driven *Cre* expression, leads to similar findings (Backman et al., 2001; Kwon et al., 2001). Taken together, our in vivo data reveal that *Pten* KI mice have an exacerbated tumor spectrum and PHTS features compared to *Pten*$^{+/-}$ mice.

Pten KI Mice Show Higher Sensitivity to Growth Factor Stimulation and Increased Akt Activation

To investigate the molecular basis of the augmented tumorigenesis observed in *Pten* KIs versus *Pten*$^{+/-}$ mice, we monitored downstream effectors of Pten. For this, we isolated primary mammary epithelial cells (MECs) from young *Pten*$^{+/+}$, *Pten*$^{+/-}$, *Pten*$^{C124S/+}$, and *Pten*$^{G129E/+}$ female mice to examine levels of Akt phosphorylation. Importantly, while *Pten*$^{+/-}$ derived MECs had increased phospho-Akt levels compared to wild-type cells, lysates from *Pten*$^{C124S/+}$ and *Pten*$^{G129E/+}$ derived MECs displayed levels of Akt activation consistently higher than those found in *Pten*$^{+/-}$ (Figures 5A and 5B). We next examined Akt phosphorylation in preonset mammary glands of 10- to 12-week-old mice by immunohistochemical staining (IHC) and found that *Pten* KI mice presented the strongest signal (Figure 5C), which persisted in tumor lesions of older mice (Figures S3G and S4C).

To further test the propensity of Pten mutations to induce Akt hyperactivation, we generated mouse embryonic fibroblasts (MEFs). Insulin-like growth factor (IGF) stimulation led to acute Akt phosphorylation in *Pten*-KI-derived MEFs, again much higher than in *Pten*$^{+/-}$ cells (Figure 5D). Similar results were observed upon insulin stimulation (Figure S5A). In addition, by monitoring the activation profile over time, we found that after 1 hr of insulin stimulation, *Pten* KI MEFs sustained higher levels of phospho-Akt (Figure 5E).

We next examined cellular levels of PIP3, which is mainly found on the leading edges of filopodia and lamellipodia, to stimulate cell migration and invasion (Kölsch et al., 2008). In MEFs, IF experiments showed that 1 min of insulin stimulation led to PIP3 accumulation at the membrane of all samples, with *Pten* KI MEFs showing the strongest signal (Figure 5F).

(E) Fractions of PTEN dimers purified as in (D), plus GST-PTENWT alone were purified. Catalytic activity of PTEN dimers was tested in phosphatase assays using PIP3 as substrate. PO4 released is normalized over levels of His-PTEN pulled down and is shown relative to the PO4 released by GST-PTENWT alone. Mean values of triplicate wells with associated SD are shown.

(F) Sequencing of Pten-*exon5* amplified from DNA of targeted ES cells. Electropherograms show expression of both Pten*wt* and Pten mutated alleles (top: *C124S*, *T-to-A*; bottom: *G129E*, *G-to-A*).

(G) Analysis of Pten protein levels. Total lysates of MEFs and adult tissues (lung and spleen) derived from *Pten*$^{+/+}$, *Pten*$^{+/-}$, *Pten*$^{C124S/+}$, and *Pten*$^{G129E/+}$ mice were resolved by SDS-PAGE. Pten quantification is normalized to β-actin and relative to WT band.

(H) Nuclear versus cytoplasmic fractionation of MEFs. Comparable distribution of Pten was observed across the different genotypes.

(I) Pten IF in MEFs: 120 cells per field (200× magnification) were scored on average. Percentage of Pten accumulation in the nucleus versus cytoplasm (at the membrane and in the cytosol) is shown with associated SD.

(J) Representative IF showing endogenous nuclear (white arrowheads) and cytoplasmic (red arrowheads) distribution of Pten in MEFs. Scale bars represent 50 μm.

See also Figure S3.

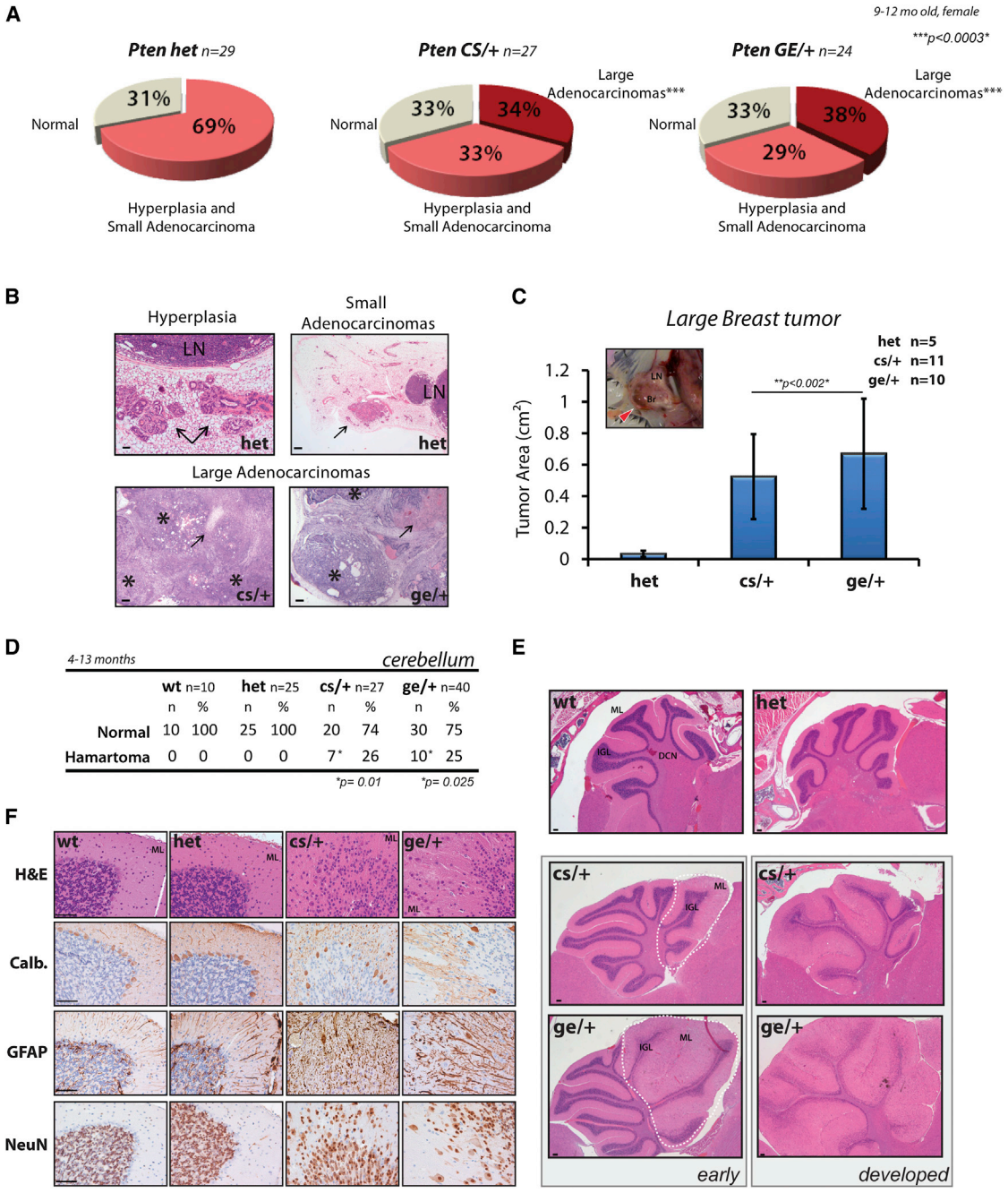

Figure 4. Dominant-Negative Effect of PTEN Cancer-Associated Mutations Leads to Enhanced Tumorigenesis and Development of Hamartoma Features

(A) Pie charts showing breast tumor distribution in *Pten*$^{+/-}$, *Pten*$^{C124S/+}$, and *Pten*$^{G129E/+}$ female mice between 9 and 12 months of age.

(B) H&E staining of tumoral lesions found in breast tissues of *Pten* mouse lines. Top: arrows point to hyperplasia (left) and small adenocarcinomas (right) found in the 68.9% of *Pten*$^{+/-}$ mice (n = 20 out of 29); LN, lymph nodes. See also Figures S3E and S3F. Bottom: sections of large breast adenocarcinomas developing in 34% of *Pten*$^{C124S/+}$ mice (n = 9 out of 27), left, and 37.5% of *Pten*$^{G129E/+}$ mice (n = 9 out of 24), right. Asterisks indicate areas of epithelial expansion surrounded by connective tissue. Arrows point to areas of necrotic tissue found in the middle core of the tumors. Scale bar represents 1 mm in hyperplasia sample, top left; and 500 μm in the remaining panels.

(C) Tumor area of large breast adenocarcinomas found in *Pten* KI mice. Inset: picture of large breast tumor (red arrowhead) developing in the inguinal fat-pad of a 9-month-old *Pten*$^{C124S/+}$ female mouse. Histogram shows average tumor area measured on paraffin blocks samples (side × side). Br, breast; LN, lymph node. Mean values with associated SD are shown.

(D) Lhermitte-Duclos disease develops in the cerebellum of *Pten* KI mice. Table shows penetrance of disease in *Pten*$^{C124S/+}$ (six females and one male) and *Pten*$^{G129E/+}$ mice (three females and seven males). See also Figures S4D and S4G.

(legend continued on next page)

Next, we monitored activation levels of Akt isoforms. Out of the three, Akt1 and Akt2 are more widely expressed, and their contributions to tumorigenesis have been better characterized (Gonzalez and McGraw, 2009). Thus, we performed IP-western blot analysis on Akt1 and Akt2 and found that both proteins were hyperphosphorylated in *Pten* KI MEFs (Figures S5C and S5D). We also examined expression levels of key components of the PI3K pathway and found no changes in total levels of its upstream or downstream components (Figure 5G); nor did we find alteration in the formation of the PI3K complex (p85:p110 binding) across the *Pten* genotypes (Figure S5B).

We then monitored the activation of several Akt targets, including the mTORC1 complex. We found that upon insulin stimulation, *Pten* KI MEFs displayed increased levels of PRAS40 phosphorylation compared to $Pten^{+/-}$ cells, resulting in mTORC1 activation and faster accumulation of phospho-S6, its downstream substrate (Figures 5H, S5F, and S5G). *Pten* KI MEFs also displayed reduced levels of IRS1, probably due to negative feedback loops driven by mTORC1activation (Figure 5G) (Shah et al., 2004). We also monitored activation of Akt targets including TSC2, Foxo1, and Foxo3a, but while both Foxo proteins were more phosphorylated in *Pten* KI MEFs compared to $Pten^{+/-}$, the status of phospho TSC2 remained unchanged (Figure 5H).

Finally, we tested the status of proposed Pten protein substrates and established their potential contribution to *Pten* loss driven tumorigenesis. (Tamura et al., 1999; Zhang et al., 2011). In our experimental conditions, however, while IGF stimulation led to Akt hyperactivation, the phosphorylation status of Fak and Src were not significantly affected across the *Pten* genotypes (Figure S5E).

Dimerization and Membrane Recruitment Identify an Active Pool of PTEN In Vivo that Is Out-Competed by Mutant PTEN

We then immunopurified Pten from $Pten^{+/+}$, $Pten^{+/-}$, $Pten^{C124S/+}$, and $Pten^{G129E/+}$ MEFs and tested the respective phosphatase activity toward PIP3. We found that free phosphate production by the heterodimeric complexes was lower than that found under *Pten* heterozygous conditions. Accordingly, reduced PIP3 hydrolysis led to increased Akt phosphorylation (Figures 6A and 6B).

Because PIP3 is produced in the inner leaflet of the plasma membrane, we next analyzed Pten membrane recruitment. To this end, we coexpressed GFPPTEN WT or mutants alongside untagged PTENWT in PC3 cells and monitored the ability of the different GFPPTEN species to localize to the plasma-membrane (PM) (Figure S6A). We found that, upon starvation and serum stimulation, GFPPTEN mutant proteins showed a 12% greater concentration (on average) at the membrane than GFPPTEN WT (Figure S6B).

To verify that PTEN is present at the membrane as homo- or heterodimers, we repeated this assay by coexpressing GFPPTEN variants with mCherry-tagged PTENWT. Coexpression of mCherryPTENWT with GFPPTENWT displayed a linear accumulation of GFP and mCherry signals at the PM, with <2% intrinsic variation, likely due to different backbone plasmids. However, in coexpressing C124S or G129E-GFP variants with mCherry-PTENWT, we observed that the GFP detection at the PM was only 4% more intense than the mCherry signal (Figures 6C and S6C), suggesting that, although both mutants are recruited to the membrane more rapidly than PTEN WT, they are also able to promote enhanced mCherry-PTENWT membrane recruitment through dimerization.

In addition, co-IPs from PC3 cell-membrane fractions confirmed that MycPTENWT can bind GFPPTENWT and GFPPTEN mutants at the membrane (Figure 6D). Thus we propose that "inactive" hetero- and homodimers may displace and outcompete the function of "active" PTEN WT homodimers.

Consequence of PTEN Mutations on Loss of Heterozygosity and Akt Activation in Mouse Models and Humans

In the mouse, monoallelic loss of *Pten* leads to tumor initiation while cancer progression often selects for loss of the functional *Pten* allele (Hollander et al., 2011). Thus, we asked whether in *Pten* KI mice, the dominant-negative action of mutant over wild-type Pten protein would trigger advanced tumorigenesis also in the absence of loss of heterozygosity (LOH). We therefore performed Southern blot (SB) analysis and laser capture microdissection (LCM) on large breast adenocarcinoma samples from *Pten* KI mice. By SB we found that on average, 50% of the *Pten* KI breast samples fully retained the *Pten wt* allele (Figure S6D). To test a larger number of samples, we then performed LCM and PCR amplification on DNA extracts and found mixed genomic profiles with only one out of six $Pten^{C124S/+}$ samples (16%) displaying total LOH and two out of six $Pten^{G129E/+}$ samples (33%) presenting either partial or total LOH (Figure 6E).

Next, we examined the status of the Pten protein by IHC and found predominantly positive staining, with areas of reduced intensity in agreement with the percentage of LOH found by SB and LCM (Figure 6F). This finding argues that the dominant-negative effect of Pten mutations exerts their negative protumorigenic effects even in the absence of LOH; however, when cancer arises, intratumoral variability and accumulation of additional mutations will eventually favor focal loss of *Pten*. Thus the persistent Akt hyperactivation, as found in large adenocarcinomas (Figure S6E), leads to accelerated cancer formation, while PTEN LOH, when observed, may further favor tumor progression.

(E) H&E staining of cerebellar sections from *Pten* mouse lines. Top: histologically normal cerebellum from $Pten^{+/+}$ and $Pten^{+/-}$ mice displaying molecular layer (ML), internal granule cell layer (IGL), and deep cerebellar nuclei (DCN). Bottom: Lhermitte-Duclos disease in *Pten* KI mice present in small areas of early lesions (left) or developing through the entire cerebellum (right). See also Figure S4D. Scale bar represents 1 mm.

(F) Immunohistochemistry (IHC) of cerebellar sections from 10-month-old *Pten* mouse lines. From the top: H&E staining shows disorganized granule cells spreading into the ML. Calbindin immunostaining shows dispersion of Purkinje cells due to granule cells overgrowth (GFAP immunostaining). NeuN immunostaining identifies presence of scattered neurons. Scale bars represent 25 μm.

See also Figure S4.

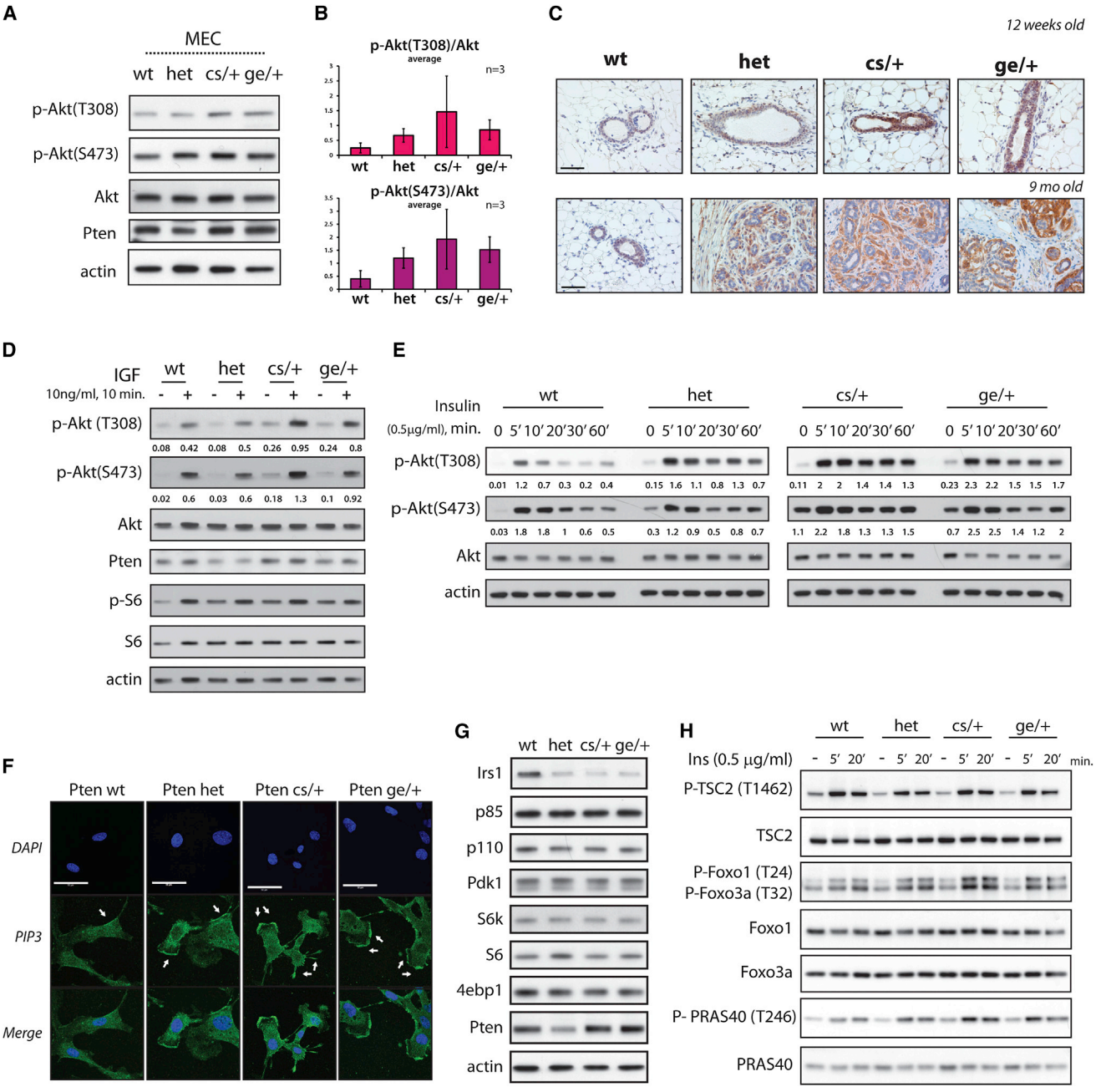

Figure 5. *Pten*$^{C124S/+}$- and *Pten*$^{G129E/+}$-Associated Tumorigenesis Is Driven by Akt Hyperactivation

(A) Total lysates of mammary epithelial cells (MECs) derived from 10- to 12-week-old female mouse lines. MECs were starved overnight and stimulated for 10 min with full serum (see Experimental Procedures).

(B) Phospho-Akt levels are normalized over total protein levels. Average of three independent experiments is shown.

(C) IHC of Phospho-Akt (S473) in breast tissue of 12-week-old female mice (top) and 9-month-old female mice (bottom). Scale bars represent 50 μm.

(D) Activation of PI3K pathway in MEFs. Total lysates were resolved by SDS-PAGE and probed with the indicated antibodies. Phospho-Akt levels are normalized over total Akt.

(E) MEFs were starved for 3 hr and stimulated with 0.5 μg/ml of insulin for the indicated time points. Phospho-Akt levels are normalized over total Akt.

(F) PIP3 immunostaining in MEFs. MEFs were starved for 3 hr, stimulated with 0.5 μg/ml of insulin for 1 min, and fixed with 4% PFA (see Experimental Procedures). Arrows point to accumulation of PIP3 at the leading edges of membrane projections. Scale bars represent 50 μM.

(G) Total lysates of MEFs were resolved by SDS-PAGE and probed to detect protein levels of members of the PI3K/Akt pathway.

(H) Activation of Akt targets in Pten-derived MEFs. MEFs were starved for 3 hr and stimulated for the indicated time points. Total lysates were resolved by SDS-PAGE and probed with the indicated antibodies.

See also Figure S5.

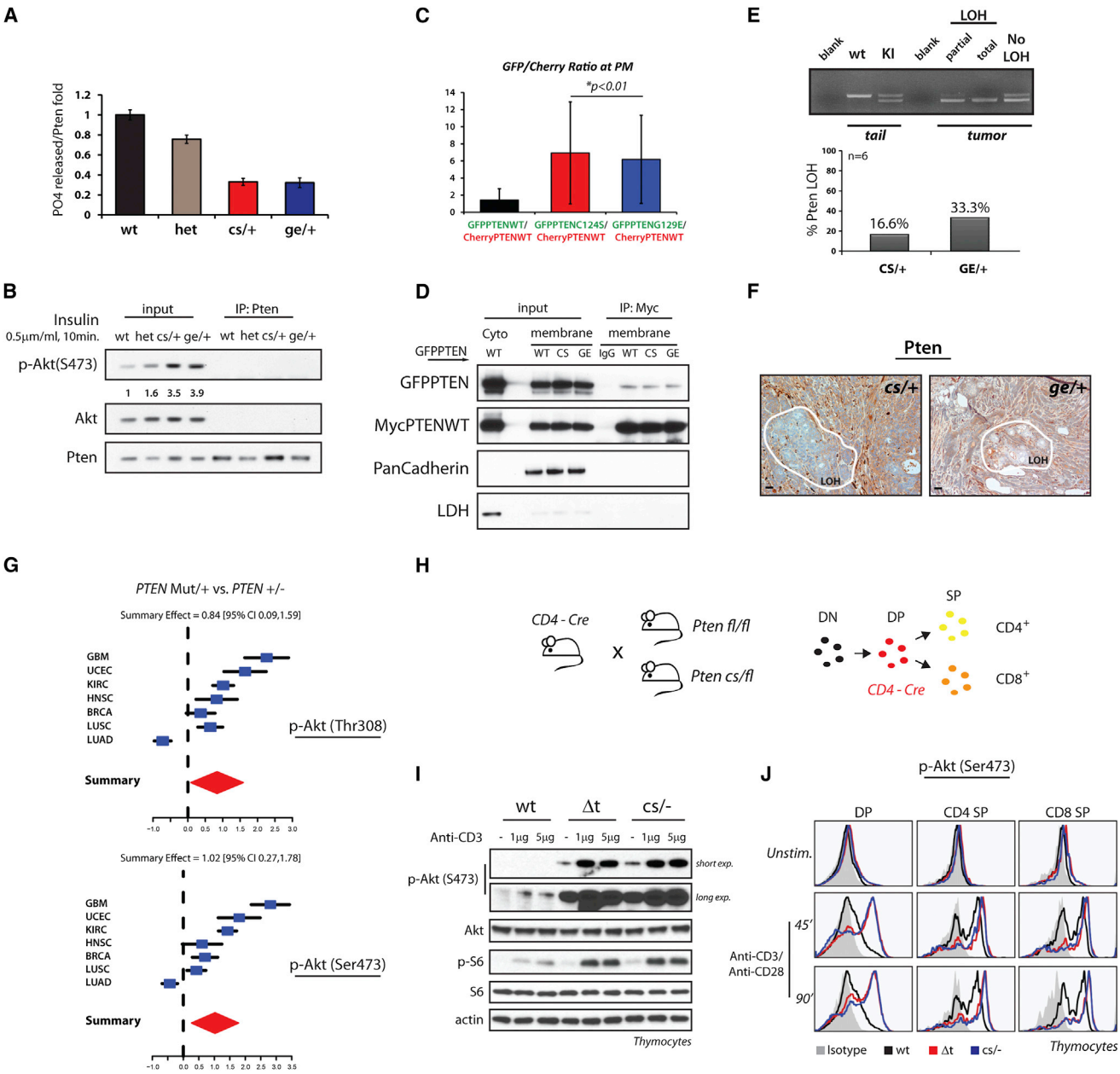

Figure 6. Akt Hyperactivation Leads to Faster Tumor Formation

(A) Analysis of Pten catalytic activity. Total lysates of MEFs were IP with an anti-Pten antibody, immunocomplexes eluted in native conditions, and relative phosphatase activity normalized over levels of Pten IP. Mean values from triplicate wells with associated SD are shown.

(B) Levels of Akt phosphorylation found in MEFs treated as in (A).

(C) PC3 cells were transfected with mCherry-PTENWT alongside GFP-PTENWT or mutants. Translocation to PM was assayed through generation of ratiometric images. Average ratios were calculated based on fluorescent intensities of mCherry and GFP species at the PM versus intensities found in the cytosol during serum reactivation. Quantification of PTEN distribution is shown.

(D) Co-IPs from membrane or cytosolic fractions of PC3 cells transfected with the indicated PTEN vectors. PanCadherin and LDH are membrane and cytosolic protein markers, respectively

(E) Laser capture microdissection (LCM) analysis performed on large breast adenocarcinoma samples of *Pten* KI mice. Top: representative PCRs of Pten *exon5* locus showing levels of *wild-type* and targeted *Pten* alleles found in microdissected breast samples. Bottom: percentage of LOH in breast tumor samples, n = 6 per genotype.

(F) IHC of large breast adenocarcinomas from 10-month-old *Pten* KI female mice. Pten expression is maintained in the majority of the breast tumor with exception of localized areas with reduced intensity (surrounded in white). LOH, area with loss of heterozygosity.

(G) Association study between *PTEN* status and AKT phosphorylation in human cancer (see Experimental Procedures). Samples harboring *PTEN* mutation are associated with higher levels of phospho-AKT(T308) (top) and phospho-AKT(S473) (bottom) compared to samples with *PTEN* heterozygosity.

(legend continued on next page)

To assess whether our observations were consistent with the molecular changes occurring in human tumorigenesis, we examined the association between PTEN mutational status and AKT activation in human cancers. For this, we analyzed data sets from The Cancer Genome Atlas available at the cBio portal (http://www.cbioportal.org) and matched the genetic status of *PTEN* with the reverse-phase protein arrays (RPPA) data for AKT. We found that samples with heterozygous mutations in *PTEN* (and no copy number alteration, including two PTENG129E mutant cases) were associated with higher levels of AKT phosphorylation (on both Thr308 and Ser473) compared to samples with heterozygous *PTEN* loss (and no additional mutations) (Figure 6G), independent of total Akt levels (Figure S6F). These data support the notion that PTEN mutations have greater consequence than heterozygous PTEN loss in promoting PI-3K/AKT hyperactivation and may predict for higher sensitivity to AKT inhibition in human cancers.

Genetic Assessment of the Dominant-Negative Role of Mutant Pten

Finally, we reasoned that, if our model was correct, then the observed differential signaling output between *Pten* KI cells versus $Pten^{+/-}$ should be absent in $Pten^{KI/-}$ versus $Pten^{-/-}$ cells. Unfortunately, this could not be addressed in MEFs because complete *Pten* loss is known to trigger cellular senescence in these cells (Chen et al., 2005); indeed, we found that $Pten^{C124S/+}$ MEFs presented increased senescence over $Pten^{+/-}$ MEFs upon passaging (Figures S6G–S6I). To overcome this problem, we made use of a conditional knockout strategy induced by the CD4-*Cre* recombinase, which is active in the double-positive lymphocyte stage of thymus development (Figure 6H). Extracted thymocytes were cultured and their PI3K-signaling output analyzed by western blot and flow cytometry analysis, respectively. Critically, in this setting we found no consistent differences in signaling output across the genotypes (Figures 6I and 6J), further supporting a model in which Pten mutations enhance PI3K/Akt oncogenic signaling by inhibiting its WT counterpart.

Functional Evaluation of PTENR130G Mutation

Because PTENC124S and PTENG129E mutations are only found in a subset of cancer and genetic syndromes, we next tested the functional role of three additional PTEN mutations more commonly found in human disease: PTENR130G, PTENR130X, and PTENR233X (Bonneau and Longy, 2000). PTENR130X and R233X nonsense mutations introduce stop codons that generate very unstable PTEN proteins that are almost undetectable (Figure S7A) and thus are functionally comparable to the *PTEN* heterozygous condition. The PTENR130G missense mutation, however, generates a stable protein that suffers loss of its lipid phosphatase function (Kato et al., 2000). In this respect, PTENR130G phenocopies PTENC124S and PTENG129E, so we further investigated its potential dominant-negative effect.

First, we confirmed that this mutation has no suppressive effect on phospho-AKT levels in PTEN null cells (Figure 7A). We next determined that PTENR130G can interact with WT PTEN in bacteria as well as eukaryotic cells (Figures 7B and 7C). Then, by testing the phosphatase function of HisPTENWT-GSTPTENR130G heterodimer purified from bacteria, we found that when bound together, PTENR130G limits the function of the WT protein to inhibit PIP3 dephosphorylation (Figure 7D). In addition, overexpression of PTEN mutations in PTEN-competent 293T cells displayed increased phospho-AKT on T308 than cells expressing empty vector, overcoming the function of endogenous PTEN (Figure 7E).

Finally, we found that samples harboring mutations on PTENR130 either mutated to Gly (R130G) or to Gln (R130Q) in a total of 19 samples from glioblastoma and endometrial cancers exhibited higher levels of AKT phosphorylation than samples with monoallelic loss of *PTEN* (Figure 7F).

DISCUSSION

In this study, we have demonstrated that PTEN dimerization is critical for its lipid phosphatase function. We have also proposed that dimeric PTEN complexes are more active than PTEN monomer in dephosphorylating PIP3 and regulating PI3K signaling. By studying two *PTEN* cancer-associated mutations, we revealed that while disrupting PTEN activity in *cis*, PTENC124S and PTENG129E inhibit the WT protein function in *trans* in a dominant-negative manner as a result of heterodimerization. In turn, this reduced Pten lipid-phosphatase activity leads to Akt hyperactivation and increased tumorigenesis in the mouse.

These findings allow us to reach several conclusions. Mechanistically, we have defined that PTEN exists as a dimer. Given that PTEN is part of the VH1-like family of DSPs, it is relevant that the prototypical VH1 phosphatase is known to exist in a dimeric-quaternary complex whose assembly is essential for the recognition of its substrate, STAT1 (Koksal and Cingolani, 2011). Moreover, phosphorylation of the PTEN tail is known to produce an inactive form of the enzyme in a closed conformation (Leslie and Foti, 2011). In agreement, we provide evidence that dephosphorylation of the PTEN-tail, while favoring a more open conformation, also allows subsequent dimerization and, possibly, oligomerization, in view of the multiple interfaces found to mediate the PTEN-PTEN interaction.

The role of PTEN dimerization in cancer is particularly important when we consider the high frequency of *PTEN* mutations in sporadic tumors and inherited syndromes. In this study, we

(H) *Pten*fl/fl and *Pten*C124S/fl mice were crossed with CD4-driven *Cre* transgenic mice (left). *Pten* deletion specifically occurs at the double-positive (DP) stage of thymocyte development. DN, double-negative thymocytes; SP, single-positive (right).

(I) Thymocytes from 3- to 4-week-old mice with the indicated genotypes were extracted and stimulated as indicated. Total lysates were resolved by SDS-PAGE and probed with the indicated antibodies.

(J) Representative flow histogram of thymocyte populations stimulated with Anti-CD3/Anti-CD28 for the indicated time. $Pten^{-/-}$ and $Pten^{C124S/-}$ thymocytes show comparable levels of phospho-Akt.

See also Figure S6.

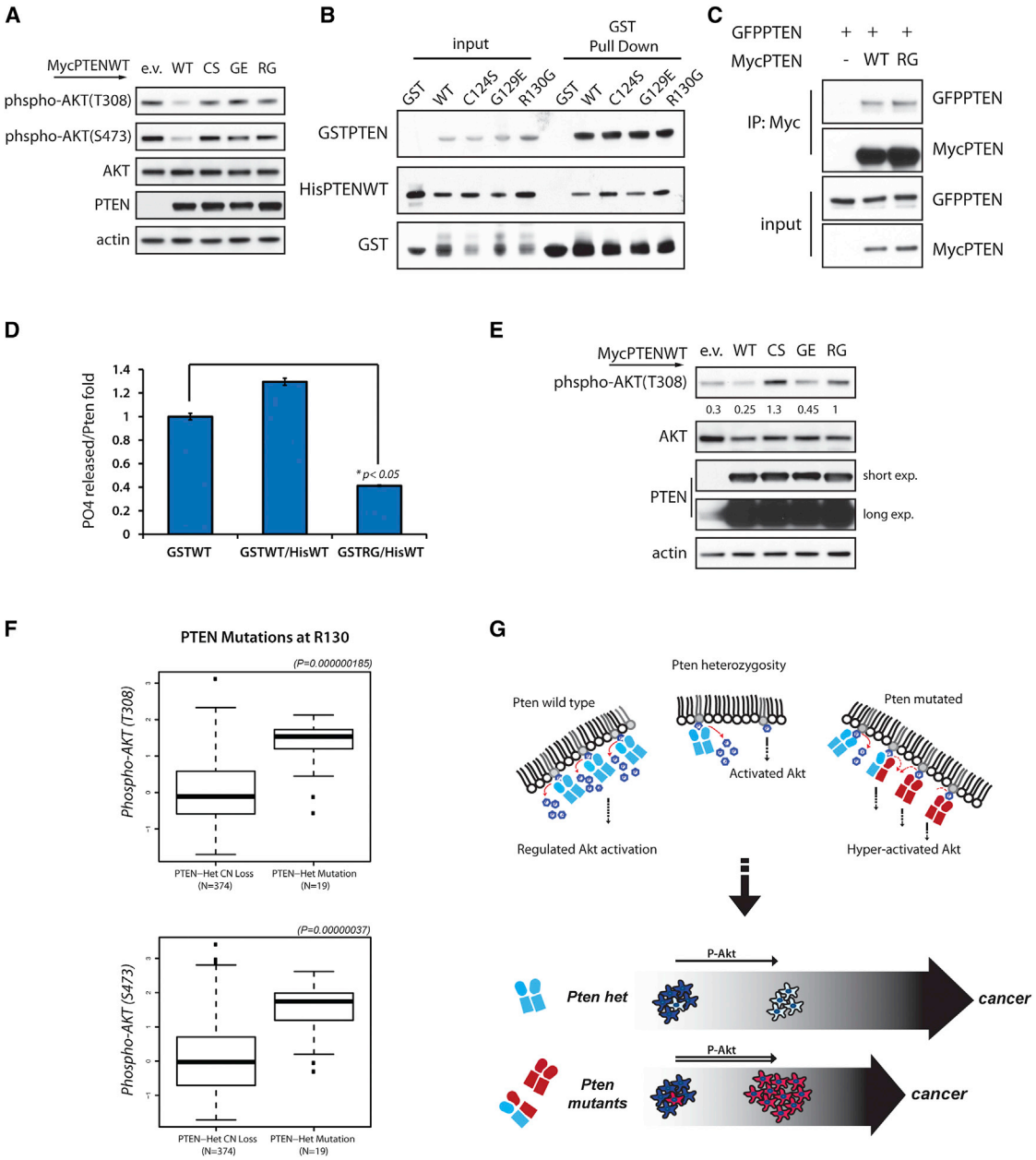

Figure 7. PTENR130G Parallels PTENC124S and PTENG129E Mutations

(A) Total lysates of PC3 cells transfected with PTEN WT and mutant expression vectors. Western blots were probed with the indicated antibodies.

(B) Bacteria were cotransformed with His-PTENWT vector alongside empty GST, GST-PTENWT, or GST-PTEN mutant vectors as indicated. Protein lysates were subjected to GST pull down and SDS-PAGE blots probed with His-tag antibody.

(C) Co-IPs from total lysates of PC3 cells transfected with the indicated vectors and IP with a Myc-tag antibody. Western blot revealed interaction between PTENWT and PTENR130G mutant protein.

(D) Phosphatase assay of PTEN dimers purified from bacteria. PO4 released is normalized over levels of His-PTEN pulled down and shown relative to the PO4 released by GST-PTENWT alone. Mean value of triplicate wells with associated SD are shown.

(E) HEK293T transfected with the indicated MycPTEN vectors were starved overnight and stimulated with 10% serum for 10 min. Total lysates were resolved by western blot and probed with the indicated antibodies. Phospho-AKT levels are normalized over total AKT.

(F) Association study between AKT activation and PTEN mutations at aa R130 in human cancers.

(G) Top: *Pten* heterozygosity leads to Akt activation and tumorigenesis. Heterozygous expression of cancer-associated *PTEN* mutations leads to formation of catalytically inactive heterodimers. Consequentially, increased PIP3 levels induce Akt hyperactivation and augmented tumorigenesis (bottom).

See also Figure S7.

have analyzed in vivo and in vitro two cancer- and CD-associated missense mutations and extended our analysis to a third mutation, PTENR130G. In the future, it will be important to study various PTEN mutations in a systematic manner. It is tempting to speculate that other PTEN mutants may affect the function of the PTEN WT protein through physical interactions and perhaps at multiple levels, e.g., by affecting PTEN extracellular export (Hopkins et al., 2013; Putz et al., 2012).

Clinically, our study implies that patients harboring these, or similar loss-of-function missense mutations, may be more susceptible to malignant cancer and may develop it more rapidly than patients expressing reduced levels of PTEN or expressing PTEN-destabilizing mutations. Thus we propose that PTEN mutational status may be utilized to stratify patients who may benefit from earlier and more radical therapeutic intervention modalities, potentially leading to improved prognoses.

Although we cannot exclude the possibility that certain PTEN mutations may become competent toward targets not recognized by the wild-type protein in a "gain-of-function" scenario (Wang et al., 2010), our genetic analyses support a model in which the ability of mutant PTEN to interfere with WT protein function contributes to exacerbation of tumor spectrum compared to *Pten* heterozygosity (Figure 7G). While these mutations induce acceleration of tumorigenesis, they specifically act by further lowering Pten activity rather than engaging alternative pathways. Accordingly, we found that *Pten* KI mice developed Lhermitte-Duclos disease, as previously reported in mice with total conditional *Pten* loss, while lesions of different histological origins not associated with *Pten* loss (such as sarcomas) were not observed.

Additionally, in monitoring the activation status of proposed PTEN phosphoprotein targets we found no obvious changes upon IGF stimulation, or variation between tumor spectra of the two *Pten* KI models. This implies that even if cancer-relevant PTEN phosphoprotein targets are present and deregulated in $Pten^{C124S/+}$ mice, concomitant Akt hyperactivation may overcome their effects, perhaps due to increased cellular senescence (Figure S6G). While several reports have highlighted the possibility that PTEN protein phosphatase activity may be related to regulation of migration and invasion (Tibarewal et al., 2012), in our in vivo analysis of the *Pten* KI mice we did not observe metastasis. However, the general exacerbation of solid tumorigenesis in multiple organs and pronounced lymphoproliferation may have masked a possible metastatic phenotype in elder mutants.

In summary, we have identified features of PTEN biology through the characterization of cancer-associated PTEN missense mutations. Given the ongoing development of agents targeting the PI3K pathway including AKT-inhibitors, our findings may help to identify patients that may be sensitive to these agents due to high levels of AKT activation associated with a PTEN mutant state.

EXPERIMENTAL PROCEDURES

Western Blotting, Immunoprecipitation, and In Vitro Binding

For details on western blotting, immunoprecipitation, and in vitro binding please refer to Extended Experimental Procedures.

Gel Filtration Chromatography

For gel filtration experiments please refer to Extended Experimental Procedures.

Mice and Immunohistochemistry

Autopsy and histological analysis was performed on cohorts of female and male mice from 2–13 months of age. Mouse tissues were fixed in 4% PFA. Normal and tumor tissues were embedded in paraffin, sectioned, and hematoxylin and eosin (H&E) stained for pathological evaluation. Brain tissues were fixed in Bouin's solution. Please refer to Extended Experimental Procedures for details on the generation of mouse lines. All mice were cared for according to NIH-approved institutional animal care guidelines and studies approved by the Institutional Committee at the Beth-Israel Deaconess Medical Center.

Studies with Primary Cells

Mouse embryonic fibroblasts (MEFs) were isolated at day E13.5 and maintained in culture as described (Todaro and Green, 1963). MEFs between passages 1 and 3 were used for all experiments. Senescence assays were performed as described (Chen et al., 2005).

Isolation of primary mammary epithelial cells (MECs) was performed as previously described (Song et al., 2013). Please refer to Extended Experimental Procedures for details.

PtdIns(3,4,5)P_3 Phosphatase Assay

PC3 cells and primary MEFs lysates from *Pten* lines were IP and subjected to native elution. For phosphatase assays, a solution with 25 mM Tris-HCl (pH 7.5), 140 mM NaCl, 1 mM DTT, and 100 μM diC_8-PtdIns(3,4,5)P_3 (Echelon) was prepared and assay ran at 37°C for 45 min. Free phosphate release was measured with Green Reagent (Biomol) and according to the manufacturer's instructions.

Population BRET Imaging

PC3 cells seeded on 35 mm wells were transfected with indicated expression vectors. After 48 hr, cells were scraped and transferred into a white OptiPlate-96 (Perkin Elmer). Luminescent emission was stimulated by adding 5 μM Coelenterazine and signal collected with the Victor3 plate reader (Perkin Elmer). Please refer to Extended Experimental Procedures for details.

Bioinformatic Analysis

We used tissue samples from The Cancer Genome Atlas (TCGA) project to assess relationships between *PTEN* mutation status, *PTEN* copy number status, and expression levels of AKT and pAKT in human cancer samples. Please refer to Extended Experimental Procedures for details.

SUPPLEMENTAL INFORMATION

Supplemental Information includes Extended Experimental Procedures and seven figures and can be found with this article online at http://dx.doi.org/10.1016/j.cell.2014.03.027.

ACKNOWLEDGMENTS

The authors would like to thank Pandolfi lab members for critical comments and Thomas Garvey for editing the manuscript. The authors are indebted to SuJung Song and Dimitrios Anastosiou for insightful discussion. A.P. was supported in part by the American-Italian Cancer Foundation Post-Doctoral Fellowship. M.B. and P.P. are supported by the Italian Association for Cancer Research (AIRC, grant number 14442). This work was supported by NIH grant U01-CA 141496 to P.P.P. L.A.T. has a family member employed by, and owns equity in, Novartis.

Received: June 11, 2013
Revised: November 25, 2013
Accepted: March 11, 2014
Published: April 24, 2014

REFERENCES

Alimonti, A., Carracedo, A., Clohessy, J.G., Trotman, L.C., Nardella, C., Egia, A., Salmena, L., Sampieri, K., Haveman, W.J., Brogi, E., et al. (2010). Subtle variations in Pten dose determine cancer susceptibility. Nat. Genet. *42*, 454–458.

Alonso, A., Sasin, J., Bottini, N., Friedberg, I., Friedberg, I., Osterman, A., Godzik, A., Hunter, T., Dixon, J., and Mustelin, T. (2004). Protein tyrosine phosphatases in the human genome. Cell *117*, 699–711.

Backman, S.A., Stambolic, V., Suzuki, A., Haight, J., Elia, A., Pretorius, J., Tsao, M.S., Shannon, P., Bolon, B., Ivy, G.O., and Mak, T.W. (2001). Deletion of Pten in mouse brain causes seizures, ataxia and defects in soma size resembling Lhermitte-Duclos disease. Nat. Genet. *29*, 396–403.

Bai, F., Pei, X.H., Pandolfi, P.P., and Xiong, Y. (2006). p18 Ink4c and Pten constrain a positive regulatory loop between cell growth and cell cycle control. Mol. Cell. Biol. *26*, 4564–4576.

Bonneau, D., and Longy, M. (2000). Mutations of the human PTEN gene. Hum. Mutat. *16*, 109–122.

Cerami, E., Gao, J., Dogrusoz, U., Gross, B.E., Sumer, S.O., Aksoy, B.A., Jacobsen, A., Byrne, C.J., Heuer, M.L., Larsson, E., et al. (2012). The cBio cancer genomics portal: an open platform for exploring multidimensional cancer genomics data. Cancer Discov. *2*, 401–404.

Chen, Z., Trotman, L.C., Shaffer, D., Lin, H.K., Dotan, Z.A., Niki, M., Koutcher, J.A., Scher, H.I., Ludwig, T., Gerald, W., et al. (2005). Crucial role of p53-dependent cellular senescence in suppression of Pten-deficient tumorigenesis. Nature *436*, 725–730.

Di Cristofano, A., Pesce, B., Cordon-Cardo, C., and Pandolfi, P.P. (1998). Pten is essential for embryonic development and tumour suppression. Nat. Genet. *19*, 348–355.

Di Cristofano, A., Kotsi, P., Peng, Y.F., Cordon-Cardo, C., Elkon, K.B., and Pandolfi, P.P. (1999). Impaired Fas response and autoimmunity in Pten+/- mice. Science *285*, 2122–2125.

Fraser, M.M., Zhu, X., Kwon, C.H., Uhlmann, E.J., Gutmann, D.H., and Baker, S.J. (2004). Pten loss causes hypertrophy and increased proliferation of astrocytes in vivo. Cancer Res. *64*, 7773–7779.

Gao, J., Aksoy, B.A., Dogrusoz, U., Dresdner, G., Gross, B., Sumer, S.O., Sun, Y., Jacobsen, A., Sinha, R., Larsson, E., et al. (2013). Integrative analysis of complex cancer genomics and clinical profiles using the cBioPortal. Sci. Signal. *6*, pl1.

Garcia-Cao, I., Song, M.S., Hobbs, R.M., Laurent, G., Giorgi, C., de Boer, V.C., Anastasiou, D., Ito, K., Sasaki, A.T., Rameh, L., et al. (2012). Systemic elevation of PTEN induces a tumor-suppressive metabolic state. Cell *149*, 49–62.

Georgescu, M.M., Kirsch, K.H., Akagi, T., Shishido, T., and Hanafusa, H. (1999). The tumor-suppressor activity of PTEN is regulated by its carboxyl-terminal region. Proc. Natl. Acad. Sci. USA *96*, 10182–10187.

Gonzalez, E., and McGraw, T.E. (2009). The Akt kinases: isoform specificity in metabolism and cancer. Cell Cycle *8*, 2502–2508.

Hollander, M.C., Blumenthal, G.M., and Dennis, P.A. (2011). PTEN loss in the continuum of common cancers, rare syndromes and mouse models. Nat. Rev. Cancer *11*, 289–301.

Hopkins, B.D., Fine, B., Steinbach, N., Dendy, M., Rapp, Z., Shaw, J., Pappas, K., Yu, J.S., Hodakoski, C., Mense, S., et al. (2013). A secreted PTEN phosphatase that enters cells to alter signaling and survival. Science *341*, 399–402.

Kato, H., Kato, S., Kumabe, T., Sonoda, Y., Yoshimoto, T., Han, S.Y., Suzuki, T., Shibata, H., Kanamaru, R., and Ishioka, C. (2000). Functional evaluation of p53 and PTEN gene mutations in gliomas. Clin. Cancer Res. *6*, 3937–3943.

Koksal, A.C., and Cingolani, G. (2011). Dimerization of Vaccinia virus VH1 is essential for dephosphorylation of STAT1 at tyrosine 701. J. Biol. Chem. *286*, 14373–14382.

Kölsch, V., Charest, P.G., and Firtel, R.A. (2008). The regulation of cell motility and chemotaxis by phospholipid signaling. J. Cell Sci. *121*, 551–559.

Kwon, C.H., Zhu, X., Zhang, J., Knoop, L.L., Tharp, R., Smeyne, R.J., Eberhart, C.G., Burger, P.C., and Baker, S.J. (2001). Pten regulates neuronal soma size: a mouse model of Lhermitte-Duclos disease. Nat. Genet. *29*, 404–411.

Lee, J.O., Yang, H., Georgescu, M.M., Di Cristofano, A., Maehama, T., Shi, Y., Dixon, J.E., Pandolfi, P., and Pavletich, N.P. (1999). Crystal structure of the PTEN tumor suppressor: implications for its phosphoinositide phosphatase activity and membrane association. Cell *99*, 323–334.

Leslie, N.R., and Foti, M. (2011). Non-genomic loss of PTEN function in cancer: not in my genes. Trends Pharmacol. Sci. *32*, 131–140.

Li, J., Lu, Y., Akbani, R., Ju, Z., Roebuck, P.L., Liu, W., Yang, J.Y., Broom, B.M., Verhaak, R.G., Kane, D.W., et al. (2013). TCPA: a resource for cancer functional proteomics data. Nat. Methods *10*, 1046–1047.

Liaw, D., Marsh, D.J., Li, J., Dahia, P.L., Wang, S.I., Zheng, Z., Bose, S., Call, K.M., Tsou, H.C., Peacocke, M., et al. (1997). Germline mutations of the PTEN gene in Cowden disease, an inherited breast and thyroid cancer syndrome. Nat. Genet. *16*, 64–67.

Maehama, T., and Dixon, J.E. (1998). The tumor suppressor, PTEN/MMAC1, dephosphorylates the lipid second messenger, phosphatidylinositol 3,4,5-trisphosphate. J. Biol. Chem. *273*, 13375–13378.

Marsh, D.J., Coulon, V., Lunetta, K.L., Rocca-Serra, P., Dahia, P.L., Zheng, Z., Liaw, D., Caron, S., Duboué, B., Lin, A.Y., et al. (1998). Mutation spectrum and genotype-phenotype analyses in Cowden disease and Bannayan-Zonana syndrome, two hamartoma syndromes with germline PTEN mutation. Hum. Mol. Genet. *7*, 507–515.

Myers, M.P., Stolarov, J.P., Eng, C., Li, J., Wang, S.I., Wigler, M.H., Parsons, R., and Tonks, N.K. (1997). P-TEN, the tumor suppressor from human chromosome 10q23, is a dual-specificity phosphatase. Proc. Natl. Acad. Sci. USA *94*, 9052–9057.

Myers, M.P., Pass, I., Batty, I.H., Van der Kaay, J., Stolarov, J.P., Hemmings, B.A., Wigler, M.H., Downes, C.P., and Tonks, N.K. (1998). The lipid phosphatase activity of PTEN is critical for its tumor suppressor function. Proc. Natl. Acad. Sci. USA *95*, 13513–13518.

Podsypanina, K., Ellenson, L.H., Nemes, A., Gu, J., Tamura, M., Yamada, K.M., Cordon-Cardo, C., Catoretti, G., Fisher, P.E., and Parsons, R. (1999). Mutation of Pten/Mmac1 in mice causes neoplasia in multiple organ systems. Proc. Natl. Acad. Sci. USA *96*, 1563–1568.

Putz, U., Howitt, J., Doan, A., Goh, C.P., Low, L.H., Silke, J., and Tan, S.S. (2012). The tumor suppressor PTEN is exported in exosomes and has phosphatase activity in recipient cells. Sci. Signal. *5*, ra70.

Ramaswamy, S., Nakamura, N., Vazquez, F., Batt, D.B., Perera, S., Roberts, T.M., and Sellers, W.R. (1999). Regulation of G1 progression by the PTEN tumor suppressor protein is linked to inhibition of the phosphatidylinositol 3-kinase/Akt pathway. Proc. Natl. Acad. Sci. USA *96*, 2110–2115.

Shah, O.J., Wang, Z., and Hunter, T. (2004). Inappropriate activation of the TSC/Rheb/mTOR/S6K cassette induces IRS1/2 depletion, insulin resistance, and cell survival deficiencies. Curr. Biol. *14*, 1650–1656.

Song, S.J., Poliseno, L., Song, M.S., Ala, U., Webster, K., Ng, C., Beringer, G., Brikbak, N.J., Yuan, X., Cantley, L.C., et al. (2013). MicroRNA-antagonism regulates breast cancer stemness and metastasis via TET-family-dependent chromatin remodeling. Cell *154*, 311–324.

Sotelo, N.S., Valiente, M., Gil, A., and Pulido, R. (2012). A functional network of the tumor suppressors APC, hDlg, and PTEN, that relies on recognition of specific PDZ-domains. J. Cell. Biochem. *113*, 2661–2670.

Suzuki, A., de la Pompa, J.L., Stambolic, V., Elia, A.J., Sasaki, T., del Barco Barrantes, I., Ho, A., Wakeham, A., Itie, A., Khoo, W., et al. (1998). High cancer susceptibility and embryonic lethality associated with mutation of the PTEN tumor suppressor gene in mice. Curr. Biol. *8*, 1169–1178.

Tamura, M., Gu, J., Takino, T., and Yamada, K.M. (1999). Tumor suppressor PTEN inhibition of cell invasion, migration, and growth: differential involvement of focal adhesion kinase and p130Cas. Cancer Res. *59*, 442–449.

Tibarewal, P., Zilidis, G., Spinelli, L., Schurch, N., Maccario, H., Gray, A., Perera, N.M., Davidson, L., Barton, G.J., and Leslie, N.R. (2012). PTEN protein phosphatase activity correlates with control of gene expression and invasion, a tumor-suppressing phenotype, but not with AKT activity. Sci. Signal. *5*, ra18.

Todaro, G.J., and Green, H. (1963). Quantitative studies of the growth of mouse embryo cells in culture and their development into established lines. J. Cell Biol. *17*, 299–313.

Trotman, L.C., Niki, M., Dotan, Z.A., Koutcher, J.A., Di Cristofano, A., Xiao, A., Khoo, A.S., Roy-Burman, P., Greenberg, N.M., Van Dyke, T., et al. (2003). Pten dose dictates cancer progression in the prostate. PLoS Biol. *1*, E59.

Vazquez, F., Ramaswamy, S., Nakamura, N., and Sellers, W.R. (2000). Phosphorylation of the PTEN tail regulates protein stability and function. Mol. Cell. Biol. *20*, 5010–5018.

Vazquez, F., Grossman, S.R., Takahashi, Y., Rokas, M.V., Nakamura, N., and Sellers, W.R. (2001). Phosphorylation of the PTEN tail acts as an inhibitory switch by preventing its recruitment into a protein complex. J. Biol. Chem. *276*, 48627–48630.

Wang, X., and Jiang, X. (2008). Post-translational regulation of PTEN. Oncogene *27*, 5454–5463.

Wang, H., Karikomi, M., Naidu, S., Rajmohan, R., Caserta, E., Chen, H.Z., Rawahneh, M., Moffitt, J., Stephens, J.A., Fernandez, S.A., et al. (2010). Allele-specific tumor spectrum in pten knockin mice. Proc. Natl. Acad. Sci. USA *107*, 5142–5147.

Zhang, S., Huang, W.C., Li, P., Guo, H., Poh, S.B., Brady, S.W., Xiong, Y., Tseng, L.M., Li, S.H., Ding, Z., et al. (2011). Combating trastuzumab resistance by targeting SRC, a common node downstream of multiple resistance pathways. Nat. Med. *17*, 461–469.